CANCOM2024 – CANADIAN INTERNATIONAL CONFERENCE ON COMPOSITE MATERIALS

ABSORPTION DOMINANT EMI SHIELDING PERFORMANCE BY LAYERED NANOCOMPOSITE/FILM STRUCTURE

Habibpour, S[1], Rahimi-Darestani, Y[1], Park, C B[2]*, Yu, A[1]*
[1] Department of Chemical Engineering, University of Waterloo, Waterloo, Canada
[2] Department of Mechanical and Industrial Engineering, University of Toronto, Toronto, Canada
* Corresponding authors (park@mie.utoronto.ca, aipingyu@uwaterloo.ca)

Keywords: *Conductive polymer Composite, MXene, Graphene Nanoribbon*

ABSTRACT

To address the ever-increasing challenges of electromagnetic pollution, there is a pressing need to develop lightweight materials with exceptional shielding capabilities. However, while previous studies have predominantly emphasized enhancing the electromagnetic interference (EMI) shielding effectiveness (SE) value, they have relatively given less attention to the absorption-dominant shielding mechanism, which holds environmental advantages by minimizing secondary pollutions. Herein, we synthesized semi-2D reduced graphene nanoribbons (rGOnR) and 2D $Ti_3C_2T_x$ MXene (MX) nanoflakes from the MWCNT and Ti_3AlC_2 MAX phase, respectively. We developed a lightweight, layered structure comprising rGOnR/MX hybridized-polydimethylsiloxane (PDMS) nanocomposite and a thin MXene film, which exhibited remarkable EMI shielding and ultra-high EM wave absorption performance. Firstly, we fabricated unidirectionally aligned aerogels of hybridized rGOnR and MXene using the freeze casting method, followed by PDMS infiltration at a low loading of 1.5 vol%. Subsequently, we constructed the layered structure by coating the nanocomposite with the MXene film. The resulting 3D interconnected network of the nanocomposite provided a tuned impedance matching layer with effective dielectric permittivity and high attenuation capability. This enabled incident EM waves to penetrate the nanocomposite and attenuate through conduction loss, polarization relaxation, and multiple scattering and reflections. Additionally, the higher conductivity MXene layer exhibited superior SE with a reflection power close to one, reflecting passed EM waves back to the nanocomposite for further attenuation. The synergistic effect of the layered structures significantly increased the total EMI SE to 54 dB over the P-band (12.4-18 GHz) at a thickness of 2.5 mm for the layered rGOnR15/MX15-PDMS nanocomposite.

1 INTRODUCTION

The rapid progress in portable electronics and telecommunications, especially with the rise of 5G technology, has significantly simplified daily life by offering faster data speeds and enabling technologies like smart cities, autonomous vehicles, and virtual and augmented reality. However, like all wireless technologies, concerns exist regarding the potential negative impacts of EMI on device functionality and human health. To mitigate these concerns, considerable efforts have been dedicated to developing advanced EMI shielding materials that are lightweight, durable, cost-effective, and easy to manufacture [1,2]. Conductive polymer nanocomposites (CPnCs) have emerged as promising materials for EMI shielding due to their lightweight properties, excellent chemical stability, ease of processing, low cost, and tunable electrical properties. These materials can be further improved for EMI shielding by enhancing interfacial polarizations, which can be achieved through the creation of varied hetero-structured surfaces using different nanomaterial combinations [3,4]. To develop EMI shielding materials with dominant absorption characteristics, it is advantageous to adjust the surface resistivity of CPnCs while reducing their

dielectric permittivity. This adjustment improves the impedance matching between the surrounding air and the shielding material, allowing incident EM waves to penetrate the material and dissipate as heat through various mechanisms such as conduction loss, polarization relaxation, and multiple scattering [5].
This research has focused on developing novel structures and materials to improve absorption dominated EMI shielding effectiveness (SE). A double-layer shielding structure has been proposed, consisting of a thin layer of highly conductive MXene film as a reflective shielding layer and a lower conductive rGOnR/MX-PDMS nanocomposite as an impedance matching layer. This structure provides excellent absorption dominant EMI SE, making it a promising candidate for future EMI shielding applications.

2 Experimental Section

2.1 Materials

Multiwalled carbon nanotubes (MWCNTs) were obtained from Cheap-Tubes Inc.. Ti_3AlC_2 MAX phase (size <40 μm), lithium fluoride, hydrochloric acid, hydrogen peroxide, phosphoric acid, sulfuric acid and potassium permanganate were purchased from Sigma Aldrich and used without further purification. Two-part PDMS (Sylgard 184) including base resin (part A) and curing agent (part B) was acquired from Dow corning Inc. and were mixed in a manufacturer recommended A:B mass ratio of 10:1.

2.2 Preparation of unidirectionally aligned aerogel based PDMS nanocomposites

GOnR and MXene were synthesized according to the procedure explained in our previous works [6,7]. To create 3D unidirectionally aligned rGOnR/MXene aerogels, a process involving directional freezing of the nanomaterial's solution followed by freeze drying was used. In a typical process, 15 mg/ml GOnR and MXene solutions were prepared and sonicated for 3 hours. The two solutions were then mixed with a total concentration of 30 mg/ml. The mixture was poured into a copper mold immersed in liquid nitrogen to induce directional growth of ice crystals. After freeze drying for 72 hours, the resulting aerogels were thermally annealed at 450°C and inert atmosphere. Similar approach was used to prepare other aerogel compositions, such as rGOnR30, hybridized rGOnR25/MX5, and rGOnR20/MX10. Aerogel based PDMS nanocomposites were prepared through the impregnation method on rGOnR/MX aerogels. After full impregnation of PDMS, the samples were placed in a convection oven at 80 °C for 4 hours to cure the polymer.

3 Results and Discussion

3.1 Material characterization

Figure 1a illustrates the large particles of the Ti_3AlC_2 MAX phase. Figure 1b is presenting exfoliated MXene nanoflakes after successful etching of the aluminum layers and the layers' delamination. Figure 1d presents the longitudinally unzipped GOnRs from their parent MWCNT illustrated in Figure 1c. Lengthwise opening of the nanotubes resulted in an increased length to width aspect ratio of the nanoribbons.

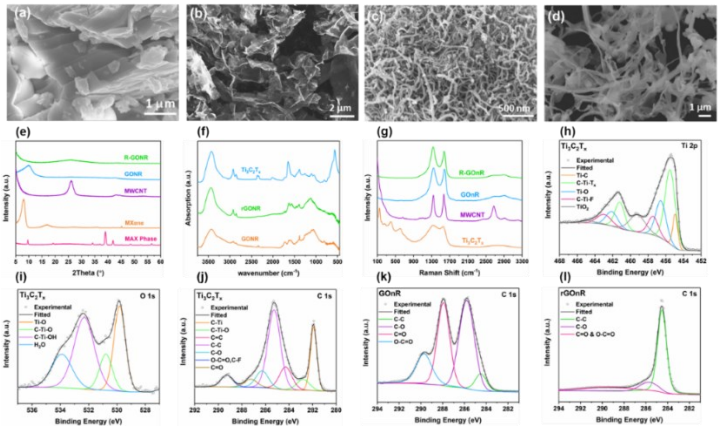

Figure 1. SEM images of (a) Ti_3AlC_2 MAX phase, (b) $Ti_3C_2T_x$ MXene, (c) MWCNT, (d) GOnR, (e) XRD, (f) FTIR, (g) Raman, and (h-l) XPS spectra of $Ti_3C_2T_x$ MXene, GOnR, rGOnR.

The changes in the crystalline structures of the nanomaterials were characterized using XRD, as shown in Figure 1e, and further analyzed with Raman and FTIR spectroscopy in Figures 1f and 1g to elucidate the integrity of the crystalline structures and functional groups. The selective removing of the aluminum layers from the MAX phase caused the characteristic peak at 2θ = 39° to disappear, broadened the peak at 2θ = 9.5°, and shifted it to a lower value of 2θ = 8°. The presence of chemical functional groups on the MXene surface was confirmed by FTIR [8]. Comparing the XRD spectra of MWCNT and GOnR revealed that the peak corresponding to the graphitic crystalline structure at 2θ = 26° shifted to a lower 2θ value of 10°. This shift indicated partial oxidation and lengthwise opening of the nanotubes through an unzipping process. The oxidation process introduced oxygen-containing functional groups, such as carboxyl and hydroxyl groups, to the edges of the opened nanoribbons. This was confirmed by the presence of a carbonyl stretching vibration bond peak at 1718 cm^{-1} in the FTIR spectrum of GOnR [9]. The chemical fingerprints of MWCNT, GOnR, and rGOnR were also explored by Raman spectroscopy and are shown in Figure 1g. The characteristic peaks of carbonaceous materials appeared at 1335, 1580, and 2680 cm^{-1}, corresponding to the D, G, and 2D modes, respectively. MWCNT showed an I_D/I_G ratio of 0.97, indicating lower structural integrity compared to the reported disorder ratio of other graphitic materials such as GnP [10]. The oxidative unzipping of the nanotubes increased the I_D/I_G ratio to 1.0, and the 2D peak disappeared.

The chemical state and atomic bonding of delaminated MXene, GOnR and rGOnR were explored by the X-ray photoelectron spectroscopy (XPS) and illustrated in Figure 1h-l. As seen from high resolution Ti 2p XPS spectra in Figure 1h, the peak at binding energy value of 454.9 eV belong to the Ti-C bond. The peaks at 455.6 and 461.2 eV were attributed respectively to the 2p3/2 and 2p1/2 of C-Ti-Tx bonds. The presence of these peaks is due to the formation of $Ti_3C_2O_x$ or $Ti_3C_2(OH)_x$ of Ti_3C_2OH-H_2O [11]. In the C1s region, deconvoluted peaks at the binding energy values of 291.9, 282.8, 284.3, 285., 286.3, 287.2 and 289.3 eV were assigned to the Ti-C, C-Ti-O, C=C, C-C, C-O, O-C=O or C-F and C=O bonds, respectively [12]. The successful reduction of nanoribbons during thermal treatment was also studied through comparing the high resolution XPS spectra of C1s regions for GOnR and its reduced rGOnR counterpart. As illustrated in Figure 1k, the peak for C-C bonds appeared at 284.5 eV. The three distinct peaks at 285.8, 287.9 and 289.7 eV were assigned to the C-O, C=O and O-C=O bonds which are indicating the generation of oxygen containing functional groups during chemical unzipping of MWCNTs [13]. These peaks were removed after thermal reduction of rGOnR.

3.2 Microstructure of aligned PDMS nanocomposites

Figure 2 illustrates both the top and side view SEM images of rGOnR/MX-PDMS nanocomposites. As it is unambiguous, all the micro pores of the aerogels were fully filled after impregnation with PDMS and there are not any remaining pores in the nanocomposites that may act as stress concentration points and impact the mechanical properties of the final nanocomposites. The lateral cross sectional SEM images of the nanocomposites clearly indicated that the highly aligned rGOnR/MX nanosheets were evenly dispersed with a particular orientation relative to the direction of the freezing [14].

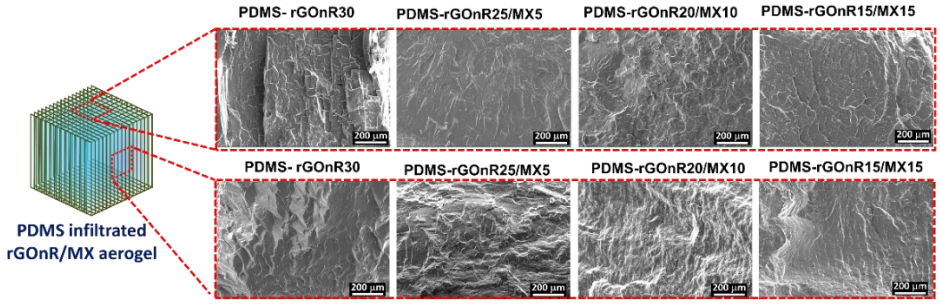

Figure 2. SEM images from the top and side view of the PDMS infiltrated rGOnR/MX aerogels

3.3 Electrical conductivity and EMI SE of nanocomposites

Linear sweep voltammetry of the PDMS nanocomposites was measured and direct current (DC) electrical conductivity of the nanocomposites were calculated using $\sigma_{DC}= t/(R\times A)$, where t is the sample thickness, A is the sample's surface area and R is the resistivity in Figure 2a. The electrical conductivity of nanocomposites showed an increasing trend with the addition of MXene nanoflakes in the structure of the aerogels. The higher electrical conductivity of the rGOnR15/MX15-PDMS nanocomposites was attributed to the synergistic effect of both graphene nanoribbons and MXene nanoflakes. EMI SE of the nanocomposites were also measured after developing a double layer structure by coating a layer of MXene film on the nanocomposites.

In theory, electrical conductivity is the key factor influencing EMI SE and the impedance matching between materials and the medium through which EM waves propagate. There is a balance to be struck between the surface electrical conductivity of the shielding material and its impedance matching with the EM wave medium. Increasing electrical conductivity can enhance EMI SE through conduction loss. However, if the electrical conductivity becomes too high, it leads to significant EM wave reflection due to impedance mismatch, which is undesirable as it may cause secondary interferences [15].

Figure 3b exhibits the thickness dependency of the average total SET of the rGOnR/MX-PDMS nanocomposites in the P-band frequency range. The SET of the coated nanocomposites increased with thickness. Furthermore, hybridizing rGOnR aerogel with MXene nanoflakes further improved the total shielding performance of the coated nanocomposites possibly due to the higher electrical conductivity devoted by the MXene nanoflakes. The average total (SE_T), reflection (SE_R) and absorption (SE_A) shielding effectiveness of the coated nanocomposites as a function of sample thickness are presented in Figure 3c-f. Absorption dominant shielding effectiveness is obtained when SE_R is less than 3.1 dB, which is associated with the absorption of more than 50% of the incident EM waves [16]. The rGOnR30-PDMS nanocomposite showed absorption dominance at a sample thickness of 3.5 mm. On the other hand, the hybridization of this material with MXene resulted in a reduction of the critical thickness of absorption dominance to 2.5 mm for rGOnR25/MX5-PDMS and rGOnR20/MX10-PDMS, and 1.5 mm for rGOnR15/MX15-PDMS nanocomposites. As the wave propagates within the material, it undergoes multiple reflections from various interfaces, leading to constructive and destructive interference patterns, depending on the thickness and composition of the material. These interference patterns ultimately result in the formation of peaks and troughs in

the reflection coefficient [17]. In addition to the multi-reflection and phase cancellation effect, the multi-reflected EM waves from the internal surfaces can interfere with the incident EM waves. This interference is due to the presence of a π/2 phase shift between the incident wave and the internal multi-reflected waves [18]. Through tuning the shielding material thickness, the above mentioned interference could either be weakened or intensified. The former results in the high reflection and the latter leads to a peak absorption mechanism. The results clearly revealed that the hybridization led to lower reflection occurring at lower nanocomposite thickness than in the non-hybridized rGOnR-PDMS nanocomposite, Figure 3g. This can be explained by the tuned surface impedance matching between the nanocomposite and air, which allows a significant portion of the incident EM waves to penetrate the material, resulting in a stronger effect of wave interference between surface reflection and rear-interface multiple reflections.

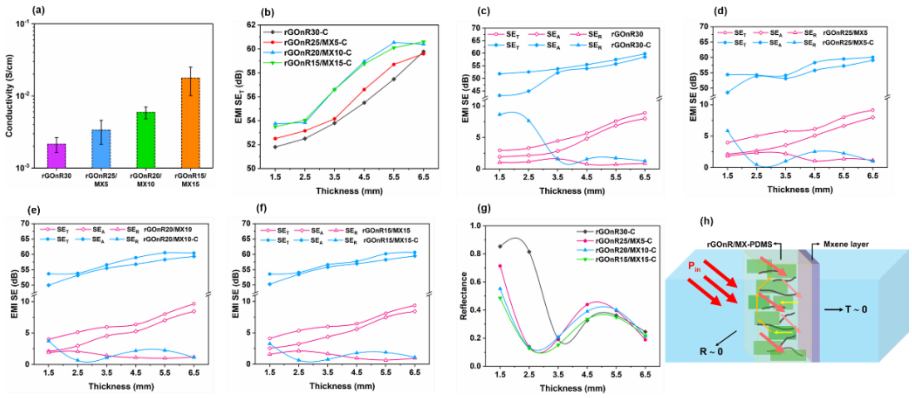

Figure 3. (a) DC electrical conductivity, (b) average EMI SE of the rGOnR/MX-PDMS nanocomposites coated with thin MXene film as a function of the specimen thickness, (c-f) average total, reflection and absorption SE of coated rGOnR/MX-PDMS nanocomposites, (g) average reflection coefficient of coated rGOnR/MX-PDMS nanocomposites as a function of thickness (h) schematic of impedance sections in series

Figure 3h depicts the mechanism of EM wave dissipation for the MXene-coated rGOnR/MX-PDMS nanocomposite developed in this study. The 3D interconnected conductive network with aligned nanomaterials optimizes the number of surface charge carriers and dielectric permittivity, reducing the impedance mismatch. This reduction allows incident EM waves to penetrate the nanocomposite rather than being reflected off the surface. Once inside, the EM waves are attenuated through various dissipation mechanisms, including: ohmic loss, inter-flake electron hopping among the aligned nanomaterials, and interfacial and dipolar polarizations at different interfaces with varying relaxation times. Any remaining EM waves reaching the highly conductive MXene layer are fully shielded and reflected due to the large impedance mismatch. These reflected waves then re-enter the 3D conductive network and, at an optimized thickness, are fully dissipated by the combined effect of all the aforementioned mechanisms.

4 Conclusions

In this study, graphene nanoribbons and MXene nanoflakes were synthesized. Using freeze casting, 3D conductive networks of rGOnR/MX aerogels were impregnated with PDMS and double layered with a thin MXene film. Hybridization of rGOnR with MXene improved the nanocomposites' electrical conductivity and dielectric properties due to MXene's higher intrinsic metallic conductivity. In double layer structure, the PDMS nanocomposites served as an absorbent layer, changing the shielding mechanism of a highly conductive MXene sheet from reflective to absorption-dominant. This hybridization reduced the minimum required thickness for absorption dominancy to 2.5 mm, attributed to tuned impedance mismatch, efficient conduction loss, and multiple reflections within the

nanocomposites. The study demonstrates how rGOnR/MXene hybridization and engineering design can enhance EMI shielding performance and change the shielding mechanism.

5 REFERENCES

[1] M. Han, D. Zhang, C.E. Shuck, B. McBride, T. Zhang, R. (John) Wang, K. Shevchuk, Y. Gogotsi, *Electrochemically modulated interaction of MXenes with microwaves*, *Nat Nanotechnol* (2023).

[2] M. Panahi-Sarmad, M. Noroozi, M. Abrisham, S. Eghbalinia, F. Teimoury, A.R. Bahramian, P. Dehghan, M. Sadri, V. Goodarzi, *A comprehensive review on carbon-based polymer nanocomposite foams as electromagnetic interference shields and piezoresistive sensors*, *ACS Appl Electron Mater* 2 (2020) 2318–2350.

[3] H. Niu, X. Tu, S. Zhang, Y. Li, H. Wang, G. Shao, R. Zhang, H. Li, B. Zhao, B. Fan, *Engineered core-shell SiO2@Ti3C2Tx composites: Towards ultra-thin electromagnetic wave absorption materials, Chemical Engineering Journal* 446 (2022) 137260.

[4] Z. Deng, P. Tang, X. Wu, H. Bin Zhang, Z.Z. Yu, *Superelastic, Ultralight, and Conductive Ti3C2T xMXene/Acidified Carbon Nanotube Anisotropic Aerogels for Electromagnetic Interference Shielding, ACS Appl Mater Interfaces* 13 (2021) 20539–20547.

[5] B. Zhao, J. Deng, C. Zhao, C. Wang, Y.G. Chen, M. Hamidinejad, R. Li, C.B. Park, *Achieving wideband microwave absorption properties in PVDF nanocomposite foams with an ultra-low MWCNT content by introducing a microcellular structure, J Mater Chem C* 8 (2020) 58–70.

[6] S. Habibpour, K. Zarshenas, M. Zhang, M. Hamidinejad, L. Ma, C.B. Park, A. Yu, *Greatly Enhanced Electromagnetic Interference Shielding Effectiveness and Mechanical Properties of Polyaniline-Grafted Ti3C2Tx MXene–PVDF Composites, ACS Appl Mater Interfaces* 14 (2022) 21521–21534.

[7] S. Habibpour, J.G. Um, Y.-S. Jun, P. Bhargava, C.B. Park, A. Yu, *Structural Impact of Graphene Nanoribbon on Mechanical Properties and Anti-corrosion Performance of Polyurethane Nanocomposites, Chemical Engineering Journal* 405 (2021).

[8] M. Naguib, M. Kurtoglu, V. Presser, J. Lu, J. Niu, M. Heon, L. Hultman, Y. Gogotsi, M.W. Barsoum, *Two-dimensional nanocrystals produced by exfoliation of Ti3AlC2, Advanced Materials* 23 (2011) 4248–4253.

[9] D.C. Marcano, D. V. Kosynkin, J.M. Berlin, A. Sinitskii, Z. Sun, A. Slesarev, L.B. Alemany, W. Lu, J.M. Tour, *Improved synthesis of graphene oxide, ACS Nano* 4 (2010) 4806–4814.

[10] J.G. Um, Y.S. Jun, A. Elkamel, A. Yu, *Engineering investigation for the size effect of graphene oxide derived from graphene nanoplatelets in polyurethane composites, Canadian Journal of Chemical Engineering* (2019) 1–13.

[11] R. Kang, Z. Zhang, L. Guo, J. Cui, Y. Chen, X. Hou, B. Wang, C. Te Lin, N. Jiang, J. Yu, *Enhanced Thermal Conductivity of Epoxy Composites Filled with 2D Transition Metal Carbides (MXenes) with Ultralow Loading, Sci Rep* 9 (2019) 1–14.

[12] J. Zhang, N. Kong, S. Uzun, A. Levitt, S. Seyedin, P.A. Lynch, S. Qin, M. Han, W. Yang, J. Liu, X. Wang, Y. Gogotsi, J.M. Razal, *Scalable Manufacturing of Free-Standing, Strong Ti3C2Tx MXene Films with Outstanding Conductivity, Advanced Materials* 32 (2020).

[13] Y.S.Y.-S. Jun, M.G.G. Park, J.G.G. Um, S. Habibpour, S. Sy, C.B.B. Park, A. Yu, *The conductivity of polydimethylsiloxane/graphene nano-ribbon foam composite with elongation, Carbon* N Y 162 (2020) 328–338.

[14] S. Zhao, H. Bin Zhang, J.Q. Luo, Q.W. Wang, B. Xu, S. Hong, Z.Z. Yu, *Highly Electrically Conductive Three-Dimensional Ti3C2Tx MXene/Reduced Graphene Oxide Hybrid Aerogels with Excellent Electromagnetic Interference Shielding Performances, ACS Nano* 12 (2018) 11193–11202.

[15] L. Ma, M. Hamidinejad, L. Wei, B. Zhao, C.B. Park, *Absorption-dominant EMI shielding polymer composite foams: Microstructure and geometry optimization, Materials Today Physics* 30 (2023).

[16] U. Hwang, J. Kim, M. Seol, B. Lee, I.K. Park, J. Suhr, J. Do Nam, *Quantitative Interpretation of Electromagnetic Interference Shielding Efficiency: Is It Really a Wave Absorber or a Reflector?, ACS Omega* 7 (2022) 4135–4139.

[17] M. Peng, F. Qin, *Clarification of basic concepts for electromagnetic interference shielding effectiveness, J Appl Phys* 130 (2021) 225108.

[18] G. Xiong, Z. Yu, J.-S. Wang, L. Zhang, *Phonon quarters-wave loss, New J Phys* 21 (2019) 093046.